PHOTONICS Research

Near-infrared electroluminescence of AlGaN capped InGaN quantum dots formed by controlled growth on photoelectrochemical etched quantum dot templates

Xiongliang Wei,[1,*] Syed Ahmed Al Muyeed,[1] Haotian Xue,[1] Elia Palmese,[1] Renbo Song,[1] Nelson Tansu,[2,3,4] and Jonathan J. Wierer, Jr.[1,5]

[1]Center for Photonics and Nanoelectronics, Department of Electrical and Computer Engineering, Lehigh University, Bethlehem, Pennsylvania 18015, USA
[2]School of Electrical and Electronic Engineering, The University of Adelaide, Adelaide, SA 5005, Australia
[3]Institute for Photonics and Advanced Sensing, The University of Adelaide, Adelaide, SA 5005, Australia
[4]e-mail: nelson.tansu@adelaide.edu.au
[5]e-mail: jjwierer@ncsu.edu
*Corresponding author: xiw314@lehigh.edu

Received 23 August 2021; revised 24 October 2021; accepted 25 October 2021; posted 28 October 2021 (Doc. ID 441122); published 9 December 2021

Near-infrared electroluminescence of InGaN quantum dots (QDs) formed by controlled growth on photoelectrochemical (PEC) etched QD templates is demonstrated. The QD template consists of PEC InGaN QDs with high density and controlled sizes, an AlGaN capping layer to protect the QDs, and a GaN barrier layer to planarize the surface. Scanning transmission electron microscopy (STEM) of Stranski–Krastanov (SK) growth on the QD template shows high-In-content InGaN QDs that align vertically to the PEC QDs due to localized strain. A high-Al-content $Al_{0.9}Ga_{0.1}N$ capping layer prevents the collapse of the SK QDs due to intermixing or decomposition during higher temperature GaN growth as verified by STEM. Growth of low-temperature (830°C) p-type layers is used to complete the p-n junction and further ensure QD integrity. Finally, electroluminescence shows a significant wavelength shift (800 nm to 500 nm), caused by the SK QDs' tall height, high In content, and strong polarization-induced electric fields.

https://doi.org/10.1364/PRJ.441122

1. INTRODUCTION

Quantum dot (QD) light emitters have great potential for light-emitting diodes (LEDs) and lasers for end-use applications such as solid-state lighting and displays [1–4]. QDs are synthesized either epitaxially [5,6] or in free-standing, colloidal form [7–10]. Of interest here are epitaxially grown InGaN QDs. Theoretically, QD-based LEDs should have a larger spontaneous emission rate than quantum well (QW) LEDs [11]. Also, QD-based laser diodes should have lower threshold currents due to low carrier thresholds and higher differential gain [12,13]. The benefits of the QD active layer for both LEDs and lasers are mainly due to the strong three-dimensional confinement of electron and holes pairs [14,15], high delta density of states, higher electron and hole wave function overlap, and lower Auger recombination at high carrier densities [4]. There are various electroluminescence (EL) demonstrations of InGaN-based QD LEDs [16–18] and lasers [19,20].

Even though QDs have compelling advantages, InGaN-based QD light emitters have lower efficiencies than QWs because of growth challenges. The traditional method is Stranski–Krastanov (SK) growth, which relies on the spontaneous formation of QDs due to the strain of the underlying growth layers. It is challenging to synthesize InGaN QDs with high dot density and uniform size distribution using SK growth, attributed to the small lattice constant difference between InGaN QDs and GaN [21–24]. Another complication is that SK InGaN QDs are not stable at high temperatures and collapse into GaN barriers via In intermixing or decomposition [25–27] due to strain between the InGaN and GaN. This instability restricts the growth temperatures of subsequent layers, such as GaN barriers. The typical growth temperature of SK InGaN QDs is between 600°C to 800°C [25,28,29], and growth temperatures of subsequent GaN barrier layers are restricted to below 800°C [27,30–32]. This low-temperature

GaN will have high defect density and poor morphology, which complicates the growth of multiple QD layers. There is a trade-off between QD integrity and high temperature grown (or higher quality) subsequent layers.

An alternative InGaN QD synthesis method is photoelectrochemical (PEC) etched QDs [33–35]. PEC QDs are formed by etching an InGaN thin film with a laser source. QDs are created from this InGaN layer during etching, and etching ends when the QDs can no longer absorb the laser light. PEC QDs have higher dot density and smaller size variations compared to SK QDs. However, the photoluminescence (PL) of PEC QDs (emission at ~445 nm), even after the surface passivation regrowth, is weaker than that of SK QDs due to surface defects [35].

It has been shown that instead of using PEC InGaN QDs as the light active layer, they can be used as a template layer for SK InGaN QD growth. SK QDs grown on PEC QD templates can have higher dot density and more controlled size distribution by growing on PEC etched InGaN QD templates due to the lattice strain from the PEC QD layer [36]. This method also avoids exposure of the light-producing QDs. PEC QDs are capped with AlGaN/GaN layers to protect the QDs and planarize the surface to complete the template. These SK QDs are intended as the light-emitting active layer in the LED.

In this work, insights and innovations are applied to SK InGaN QDs grown on PEC QD templates. AlGaN capping layers are employed to prevent collapse via In intermixing or decomposition of InGaN QDs and enable higher GaN barrier growth temperatures [37,38]. This capping scheme removes the trade-off between QD integrity and GaN barrier growth temperature. Different Al-content AlGaN capping layers are studied to protect the SK and PEC QDs against collapse at different GaN barrier growth temperatures. Atomic force microscopy (AFM) and scanning transmission electron microscopy (STEM) show the structure of QDs at various growth steps. These measurements show that high-Al-content $Al_xGa_{1-x}N$ ($x = 0.9$) capping layers prevent SK QDs from collapsing and conclusively prove that SK QDs vertically align to PEC QDs due to localized strain. A low-temperature p-type GaN layer is grown on the top of the intact SK InGaN QDs to protect them from high temperatures and complete the p-n junction to perform EL measurements. These QD-based LEDs are dominated by SK QD emission and exhibit a large wavelength blueshift from 800 nm to 500 nm with increased applied voltage, caused by the high indium content, tall QD height, and large polarization-induced electric fields in SK QDs. The wavelength shift with bias matches Schrodinger–Poisson calculations of carrier screening in InGaN QDs. The QD growth control and protection methods employed here are advances to create QDs closer to ideal theoretical performance.

2. EXPERIMENTAL DETAILS

The QD samples are grown by vertical-flow metalorganic chemical vapor deposition (MOCVD), starting with *c*-plane planar n-type GaN on patterned sapphire substrates at a pressure of 200 Torr (1 Torr = 133.3 Pa). First, to fabricate the PEC QD templates, a 7.5 nm thick $In_yGa_{1-y}N$ thin film is grown at 730°C, resulting in emission at ~470 nm and $y \sim 0.15$. These films are etched in a PEC cell with a 0.9 V bias controlled by a potentiostat, 0.2 mol/L dilute H_2SO_4, and illuminated with a 445 nm coherent light for approximately 15 min. InGaN QDs formed by this method have a dot density of $\sim 10^{10}$ cm^2, average dot height of ~12 nm, and average diameter of ~20 nm, and emit light at 445 nm, as shown previously [35]. These PEC QDs are placed back into the MOCVD chamber to regrow a 2 nm thick $Al_{0.45}Ga_{0.55}N$ capping layer using a V/III ratio of 18,000 at 730°C and a 5 nm thick GaN barrier with a V/III ratio of 18,000 at 880°C, which completes the PEC QD template. Both the capping and barrier layer thicknesses are determined from planar growth, so they can fill in and planarize the PEC QDs.

SK QDs are grown by MOCVD on the top of the PEC QD templates with two different Al-content $Al_xGa_{1-x}N$ capping layers to demonstrate their role in protecting SK QDs against In intermixing or decomposition. First, the SK QDs are grown at 655°C for 42 s with a low V/III ratio of 4200 and an In/(In+Ga) ratio of 0.5 [29,36]. Then a 2 nm thick $Al_xGa_{1-x}N$ capping layer with $x = 0.1$ or 0.9 is grown at 655°C with a V/III ratio of 18,000. Then a 10 nm thick GaN cap barrier is grown at 855°C or 880°C with a V/III ratio of 32,000. The growth of both PEC and SK QDs is interrupted at the QD and AlGaN growth steps, and AFM and STEM are used to observe how the growth conditions affect the QDs and surface morphology. The capping and barrier layers are thick enough to fill in and planarize the SK QDs.

An SK QD sample with a 2 nm thick $Al_{0.9}Ga_{0.1}N$ capping layer and 10 nm thick GaN barrier is placed back into the MOCVD reactor to regrow p-type GaN layers with a TEGa precursor that consists of: a 10 nm thick undoped GaN layer at 880°C with a V/III ratio of 16,000; a 100 nm thick Mg-doped, p-type GaN layer grown at 830°C with a V/III ratio of 28,000 and a hole concentration of $\sim 10^{17}$ cm^{-3}; and a 5 nm thick heavily Mg-doped (p^+) GaN layer grown at 830°C with a V/III ratio of 25,000. TEGa cracks at lower temperatures than TMGa and allows for lower growth temperatures to protect the QDs and ensure smooth surfaces. Finally, circular nickel contacts 200 nm thick and 200 μm in diameter are deposited on

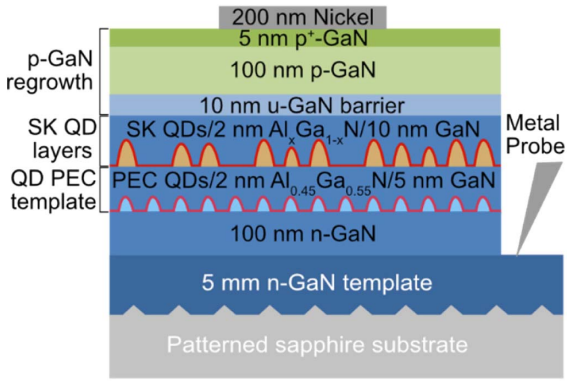

Fig. 1. Schematic cross section of the entire LED structure consisting of Stranski–Krastanov (SK) quantum dots (QDs) grown on photoelectrochemical (PEC) etched QD templates. Both QD layers are capped with AlGaN layers to protect the QDs. The p-GaN contact is formed by Ni evaporation through a shadow mask, and an electrical "flash" process creates the n-contact.

the sample by electron beam evaporation through a shadow mask. This circular contact defines the LED area because low carrier mobility prevents the current from spreading beyond its extent. The complete QD LED structure is shown in Fig. 1. Instead of forming an n-contact, an industrial quick test method is used where the n-contact is "flashed" by probing at a high voltage that causes the breakdown of the upper LED layers down to the n-type layers. The EL measurement is performed using this flashed n-contact and a second probe to contact the Ni p-contact. The LEDs are biased at various currents, and the voltage and spectra are measured.

3. RESULTS AND DISCUSSION

The integrity of PEC QDs and the eventual template morphology are determined by pausing at each step (PEC etching, AlGaN capping layer growth, and GaN barrier growth) and taking AFM images. Figure 2(a) shows an AFM image of PEC etched QDs over a 2 mm × 2 mm area. The PEC QDs are approximately 7 nm tall, the density is high, and the size distribution is relatively uniform, similar to previous reports [36]. Figure 2(b) shows an AFM image of PEC QDs with a 2 nm thick $Al_{0.45}Ga_{0.55}N$ interlayer barrier grown at 730°C and annealed at 880°C for 5 min. The growth temperature of the $Al_{0.45}Ga_{0.55}N$ capping layer is chosen to be the same temperature as the PEC QD InGaN layer (730°C) to cover and prevent the collapse of the QDs. Additional annealing is employed to replicate the temperature this structure experiences during GaN barrier growth and determine if the PEC QDs remain intact. Figure 2(b) shows that PEC QDs retain their shape and densities and are protected by the 2 nm thick $Al_{0.45}Ga_{0.55}N$ capping layer. This AFM image gives confidence that PEC QDs will not collapse during GaN barrier growth (confirmed later by STEM). Figure 2(c) shows the AFM image of the same structure as in Fig. 2(b) with the addition of a 5 nm thick GaN barrier grown at 880°C. The surface is planarized by the GaN barrier growth, with excellent step morphology and the typical small pits on the surface caused by threading dislocations from the GaN/Al_2O_3 substrate. These layers constitute the full PEC QD template used for the growth of SK QDs.

Next, SK QD samples are grown on top of PEC QD templates. The localized strain caused by PEC QDs in the template layer affects the SK QD size distribution and density [36]. The In and Ga atoms prefer to form on top of the strained area (above the PEC QDs). If the AlGaN/GaN capping layers in the template are too thick, the benefits are lost, and SK QDs grow unaffected by PEC QDs (similar to planar GaN). Figure 3(a) shows an AFM image of SK QDs with an average height of 12 nm and average radius of 40 nm. The dot density is slightly lower than that of the QD template. The SK QD growth temperature employed here is higher than previous reports [36], and there is a dependence of reduced dot density with increasing growth temperature that requires further investigation. The surface between the SK QDs is smooth with no pits, which is different from the PEC QD template surface. This AFM image is an indication that an InGaN wetting layer has covered the GaN surface.

Two different $Al_xGa_{1-x}N$ capping layers are investigated with $x = 0.1$ and 0.9 to determine the effect of Al content on QD collapse. Figure 3(b) shows an AFM image of a 2 nm thick $Al_{0.1}Ga_{0.9}N$ capping layer annealed at 880°C for 10 min to simulate the GaN barrier growth temperature and time. The AFM images show a much flatter surface and suggest that SK QDs are affected by the growth and annealing steps. The average height of the SK QDs still visible reduces significantly to 2 nm, compared to the original SK QD height of 12 nm. Finally, SK QDs are capped with a 2 nm thick $Al_{0.1}Ga_{0.9}N$ layer grown at 655°C (not annealed) and an additional 10 nm thick GaN barrier grown at 880°C. Figure 3(c) shows the AFM image where the GaN barrier recovers the flat growth surface.

Figures 3(d) and 3(e) show STEM images of QDs at a 20 nm scale and 10 nm scale, respectively. The PEC QD layer is visible as the darker layer near the bottom of the images. This layer consists of the 2 nm thick $Al_{0.45}Ga_{0.55}N$ capping layer and the InGaN QDs marked with vertical and dome-shaped lines in Figs. 3(d) and 3(e), respectively. The imaging of the QDs is not sharp because the average viewing thickness of the STEM sample is ~70 nm, while the PEC QDs have smaller diameters of ~20 nm. However, the STEM images confirm that the PEC QDs remain intact, as suggested by the AFM images in Fig. 2. SK QDs are visible as the white line above the PEC QDs, and it appears primarily continuous across the image. This STEM image along with the AFM images demonstrates that SK QDs lose their original shape and become more QW-like because the $Al_{0.1}Ga_{0.9}N$ capping layer is unable to protect SK QDs from the GaN barrier growth. This is behavior similar to GaN capped InGaN QDs [26].

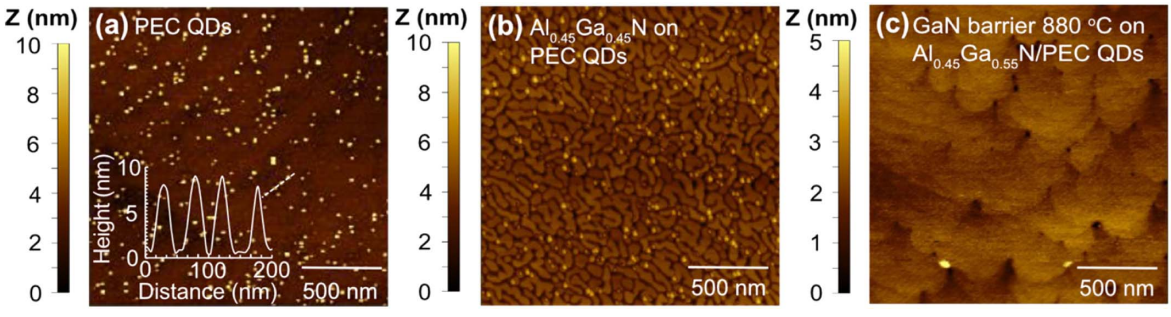

Fig. 2. Atomic force microscope (AFM) images of a PEC QD template at different synthesized steps: (a) PEC QDs after etching, (b) PEC QDs with $Al_{0.45}Ga_{0.55}N$ grown at 730°C and annealed at 880°C, and (c) PEC QDs with $Al_{0.45}Ga_{0.55}N$ grown at 730°C and GaN barrier grown at 880°C. The AFM images demonstrate that $Al_{0.45}Ga_{0.55}N$ can protect the PEC QDs against collapse.

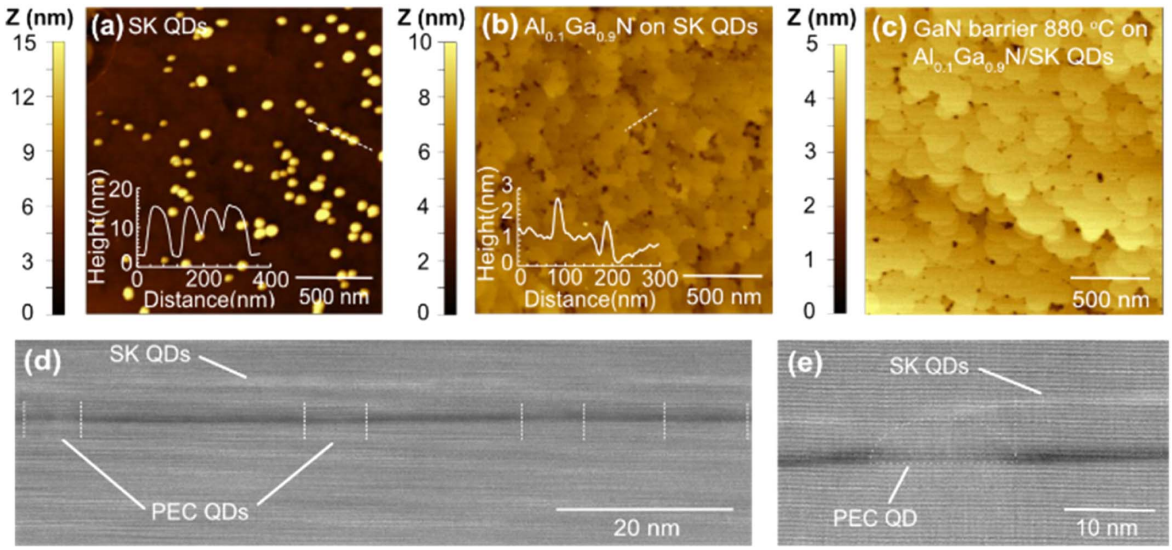

Fig. 3. AFM images of SK QDs grown on a PEC QD template and with $Al_{0.1}Ga_{0.9}N$ capping and GaN barrier layers. Surfaces of (a) SK InGaN QDs grown at 655°C, (b) SK InGaN QDs capped with $Al_{0.1}Ga_{0.9}N$ grown at 655°C and annealed at 880°C, and (c) SK InGaN QDs with an $Al_{0.1}Ga_{0.9}N$ capping layer grown at 655°C and GaN barrier grown at 880°C. STEM images at (d) 20 nm and (e) 10 nm scale. STEM images show that PEC QDs remain intact, but SK QDs collapse into a QW-like layer due to the insufficient capping and the 880°C GaN barrier growth.

The Al content of the AlGaN capping layer is increased because higher-Al-content AlGaN layers have been shown to prevent In diffusion out of InGaN layers and collapse [37]. Additionally, the GaN barrier growth temperature is decreased closer to the growth temperatures of the SK QDs. Figure 4(a) shows an AFM image of SK QDs grown on a PEC QD template capped with a 2 nm thick $Al_{0.9}Ga_{0.1}N$ layer and a 10 nm thick GaN barrier grown at 855°C. As the AFM image shows, the GaN barrier does not recover a flat surface, but the QDs exist even after GaN barrier growth. The height of the QDs is approximately 12 nm, which is almost the same as the height of the SK QDs before GaN barrier growth. It implies that SK QDs remain intact during GaN barrier growth, and the AlGaN layer effectively protects them. Figure 4(b) shows an AFM image of the sample grown the same as in Fig. 4(a), except the GaN barrier growth temperature at 880°C. The images show that the GaN barrier can cover SK QDs and produce a flat surface at this temperature.

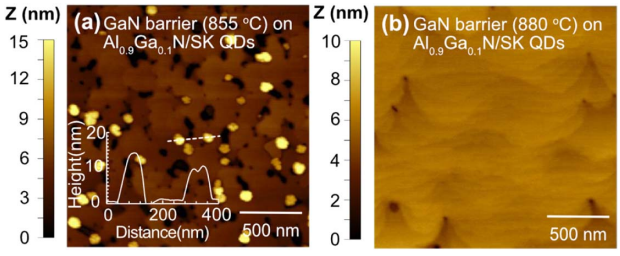

Fig. 4. AFM images of SK QDs with an $Al_{0.9}Ga_{0.1}N$ capping layer grown at 655°C and GaN barrier grown at (a) 855°C and (b) 880°C. AFM images show that at an 855°C GaN growth temperature, the $Al_{0.9}Ga_{0.1}N$ capping layer protects the SK QDs, but the following GaN barrier grows conformally on the SK QDs. The GaN barrier grown at 880°C planarizes the surface.

To confirm that the higher-Al-content AlGaN capping layer is protecting the SK QDs, STEM is performed. Figures 5(a)–5(c) show STEM images at various scales for SK QDs capped with an $Al_{0.9}Ga_{0.1}N$ layer and with the higher temperature GaN barrier. The bottom mostly black layer is PEC QDs with the $Al_{0.45}Ga_{0.55}N$ capping layer, and the top mostly black layer is the SK QD layer with the $Al_{0.9}Ga_{0.1}N$ capping layer. As the STEM image shows, both PEC and SK QDs remain intact, and the SK QDs tend to grow on top of the PEC QDs. The $Al_{0.9}Ga_{0.1}N$ capping layer is preventing In intermixing and decomposition either due to strain balancing or as a capping effect where substitution of Al and In atoms is less energetic than In and Ga atoms [37,39,40]. This STEM also shows that the SK QD growth positions are influenced by the PEC QD templates, most likely by localized strain near the QDs. Figure 5(c) is an STEM image of a single SK QD on top of a PEC QD. The height of QDs appears to be ~2.5 nm, but just like the other STEM image, the thickness of the STEM sample is much greater than the diameter of the dots, so it is impossible to assess the height with these STEM images accurately.

The lighter line visible below the SK QDs in Fig. 5 is a ~2.5 nm thick InGaN wetting layer. The energy dispersive spectroscopy (EDS) image in Fig. 5(d) confirms an $In_zGa_{1-z}N$ layer with an In-content of $z \sim 0.24$. This composition is near our growth target of $z \sim 0.25$. SK QD growth starts with an epitaxial layer, and as growth progresses, this film reaches a critical thickness and 3D growth begins. The epitaxial layer formed before the QDs is called the wetting layer and is a signature of SK QD growth. This AFM confirms that our MOCVD-grown QDs are formed via the SK method and not another QD growth technique such as Volmar–Weber growth, where QDs form immediately. Of course, this wetting layer is absent in the lower PEC QD layer because these QDs are formed by etching down to the underlying GaN.

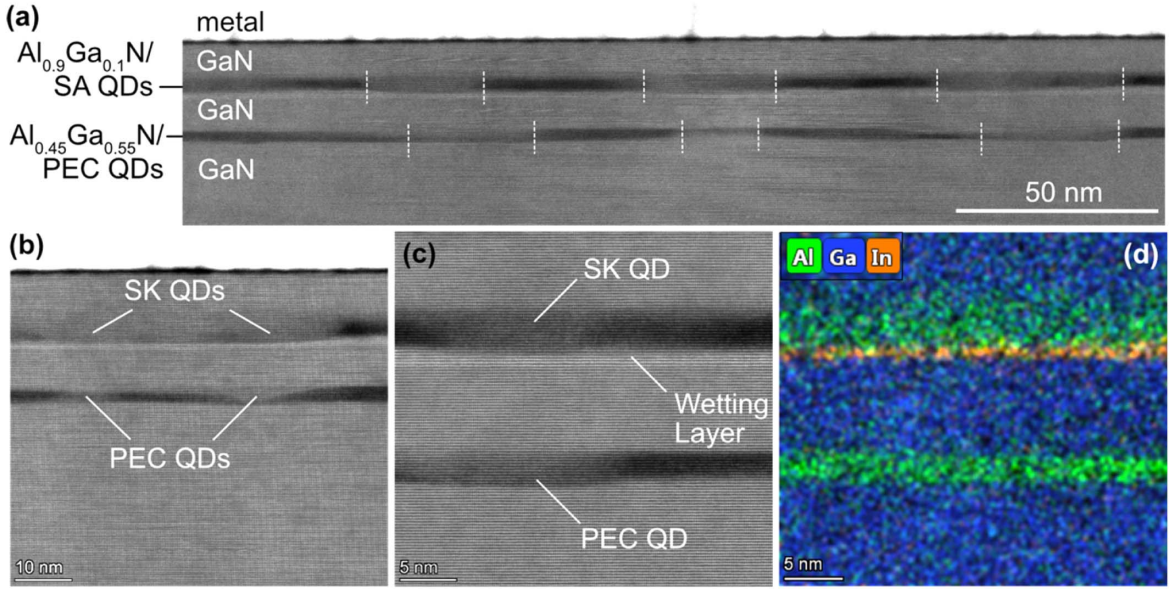

Fig. 5. STEM images of SK QDs capped with an $Al_{0.9}Ga_{0.1}N$ layer and with a GaN barrier grown at 880°C shown at (a) 20 nm, (b) 10 nm, and (c) 5 nm scale. The images show that SK QDs grow on top of the PEC QDs, and the $Al_{0.45}Ga_{0.55}N$ barrier and $Al_{0.9}Ga_{0.1}N$ barrier can protect the PEC QDs and SK QDs, respectively, from collapse at the 880°C growth temperature. (d) EDS image of the sample showing the existence of a wetting layer (orange) below the SK QDs.

The sample in Fig. 5 is returned to the MOCVD chamber to regrow p-type GaN layers and complete the p-n junction for EL measurements. Figure 6(a) shows the light output power, external quantum efficiency (EQE), and voltage versus current characteristic for this QD LED. The current increase (sometimes called threshold voltage) is <2 V and is much lower than that of a typical $In_{0.25}Ga_{0.75}N$ QW LED but is consistent with the long emission wavelength shown below. It also has a good differential resistance of ~25 Ω at higher currents, which are expected given the device size. The power of the QD light emitter increases across the measured current range, and the QDs are not saturated. The wetting layer may be aiding in injecting carriers into the QDs via QW to QD tunneling [41], but this requires further study. The EQE of the LED has a linear increase at low current densities, and then it starts to saturate in the high current density range. There is no visible drop in efficiency (droop) at the measured currents. A complete radiative analysis is required to quantitively determine whether suppressed Auger recombination, enhanced spontaneous emission, high Shockley–Read–Hall recombination, or leakage currents are causing this droop-less EQE characteristic.

Figure 6(b) shows the spectrum of the QD LEDs at different currents. The inset is the spectrum of the QD LED in a linear scale, and the full width at half maximum is 86 nm at 150 mA. A significant peak wavelength shift is observed from 800 nm to 500 nm as the current increases from 2 mA to 150 mA. Currents above 150 mA (~475 A/cm^2) lead to breakdown of QD LEDs due to limitations of the simple test structure, leakage currents, and heating. The near-infrared wavelength can be emitted only from SK QDs because PEC QDs emit closer to the etch laser wavelength of 445 nm [35], and the wetting layer is too thin (2.5 nm) and the In content is

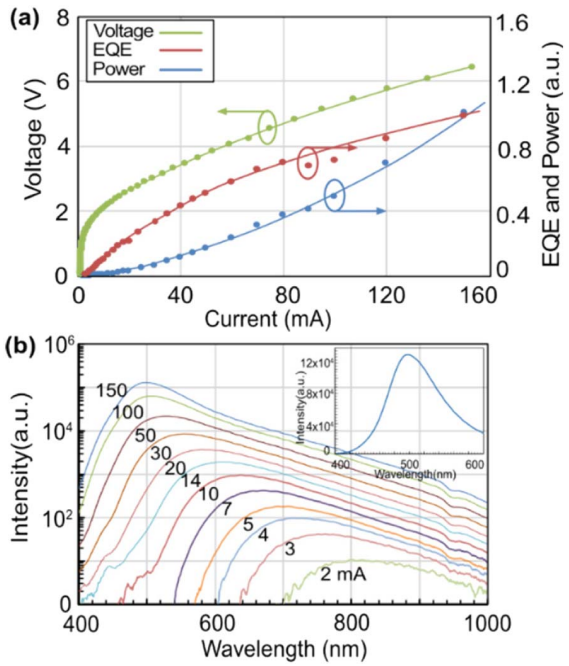

Fig. 6. Electroluminescence measurement of the QD LED. (a) Voltage, external quantum efficiency (EQE), and light power versus current of the QD LED. The threshold voltage is <2 V, and the differential resistance is ~25 Ω. As the current increases, the EQE increases linearly at low current density and slows down at high current density. (b) Spectrum of the QD LED under different currents. The wavelength blueshifts from 800 nm to 500 nm as the current increases. The inset is the spectrum in a linear scale demonstrating a full width at half maximum of 86 nm at 150 mA.

too low to produce these long wavelengths. QDs have an average height of 12 nm compared to the conventional QW, typically 2 nm to 3 nm thick. LEDs are stable, and no degradation in light output is observed during testing.

The wavelength shift can be explained in the following way. III-nitrides are polar materials, and a lattice mismatch between dissimilar alloys leads to spontaneous and piezoelectric polarization. So, the larger thickness of QDs, compared to QWs, leads to stronger polarization-induced electric fields, causing a large tilt in the QD energy bands. The tilt causes a redshift in the transition and a spatial separation in the electron and hole overlap compared to flat bands. As the current increases, the polarization-induced electric field is screened by the charged carriers, and the energy transitions blueshift. Increased currents and carrier screening also result in improved spatial overlap of electrons and holes, increasing the radiative recombination rate and overall efficiency.

To confirm that carrier screening is causing the blueshift, three-dimensional Schrodinger–Poisson simulations of a single QD are performed. The inset of Fig. 7(a) shows that the simulated $In_{0.25}Ga_{0.75}N$ QD is hexagonal, and 12 nm in height, 48 nm in the long base axis, and 34 nm in the long top axis. The top and sides of the QD are covered in a 2 nm thick $Al_{0.9}Ga_{0.1}N$ layer, and this structure is surrounded by GaN. In the simulation flow, the strain, polarization charges, and electrical field are calculated first. Then the Schrodinger equation is used to calculate the three-dimensional wave functions and energy levels of the ground states. Carrier screening is simulated by adding interface charges at the AlGaN/GaN, GaN/InGaN, and AlGaN/InGaN interfaces at various fractions and opposite signs to counter the polarization charges. The applied interface charge densities vary from 0 to 3.4×10^{13} cm^{-2}. The full piezoelectric and spontaneous polarization parameters used in the simulation are from Ref. [42] except for the elastic coefficient, e_{15}, from Ref. [43].

Figure 7(a) shows the emission wavelength of the ground energy transition and the overlap of the electrons and holes wave function versus carrier screening. The unscreened emission wavelength is at ~880 nm, and it blueshifts with increased carrier screening. The completely screened QD emits at ~500 nm. The wavelengths and blueshift in the simulation match the QD LED EL, confirming that the wavelength shift can be explained by polarization and carrier screening. As the carrier screening increases, the electrons and holes wave function overlap squared increases by six orders of magnitude, which shows the dramatic carrier screening effect in the tall QDs. Figures 7(b) and 7(c) are the vertical cross sections of the band diagrams of QDs at 100% screening and 0% screening, respectively. At 0% carrier screening, the electrons and holes are separated by the polarization charges. Since the QD is tall, the overlap of the electron and hole wave function is small, and the band structure of the QD is tilted significantly, which leads to weak near-infrared light emission of the QD LED at low carrier density. At 100% carrier screening, no band bending exists in the QDs, and the electrons and holes are centered in the QD with a high wave function overlap squared. Methods to reduce the wavelength blueshift in the QD LED as current increases are similar to QWs, and include growing QDs on semi-polar or non-polar planes, or growing smaller-sized QDs.

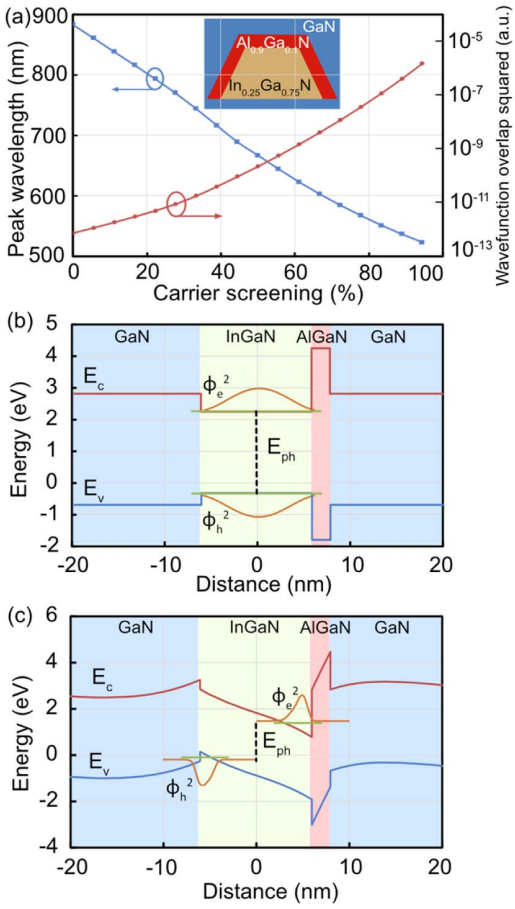

Fig. 7. (a) Simulated peak wavelength and wave function overlap squared of the ground state transitions versus carrier screening for a single $In_{0.25}Ga_{0.75}N$ QD capped with a 2 nm thick $Al_{0.9}Ga_{0.1}N$ layer. The QD is hexagonal in shape and surrounded by GaN. The peak wavelength blueshifts with increased carrier screening. Band diagrams and wave functions squared in the vertical direction through the center of the QD for (b) 100% and (c) 0% carrier screening. The wave functions shift from the top and bottom of the QD with no screening to the center with full carrier screening.

It should be noted that it is challenging to achieve near-infrared emission from InGaN QWs. The thickness and In content necessary in a QW are well beyond strain limitations, and attempting to grow such a structure would result in poor material quality and prohibit any emission. The QDs demonstrated here obviously have relaxed constraints. Their smaller lateral sizes allow for taller structures due to relaxed strain limitations, and the capping layer helps retain In in the QD. Therefore, QDs are a pathway to longer wavelength emission in InGaN materials such as efficient red emitters, useful in application such as solid-state lighting or displays.

4. CONCLUSION

A QD LED is demonstrated using a PEC etched QD template to control the growth of SK QDs and AlGaN capping layers to protect the QDs. The AlGaN capping layer with high Al

content protects the InGaN QDs against collapse and allows the GaN barrier to be grown at higher temperatures (880°C). STEM images of SK QDs formed on PEC QD templates with $Al_{0.9}Ga_{0.1}N$ capping layers show that SK QDs grow vertically on the top of PEC QDs. This alignment is evidence that the strain from the underlying PEC QD layer affects the growth of SK QDs and their size distribution and density. Finally, EL of the QD LED shows a significant wavelength shift from the near-infrared to green. The long-wavelength emission and large blueshift are an indication that the light is emitted from SK QDs, as supported by simulations.

Funding. National Science Foundation (1708227, 1935295, ECCS-2025064); Daniel E. '39 and Patricia M. Smith Endowed Chair Professorship Fund.

Acknowledgment. The MOCVD growth and LED fabrication were performed at Lehigh University's Integrated Nanofabrication and Cleanroom Facilities. The STEM in Fig. 5 was performed at the Analytical Instrumentation Facility (AIF) at North Carolina State University, which is supported by the State of North Carolina and the National Science Foundation. The AIF is a member of the North Carolina Research Triangle Nanotechnology Network (RTNN), a site in the National Nanotechnology Coordinated Infrastructure (NNCI).

Disclosures. The authors declare no conflicts of interest.

Data Availability. Data underlying the results presented in this paper are not publicly available at this time but may be obtained from the authors upon reasonable request.

REFERENCES

1. Z. Liu, C.-H. Lin, B.-R. Hyun, C.-W. Sher, Z. Lv, B. Luo, F. Jiang, T. Wu, C.-H. Ho, H.-C. Kuo, and J.-H. He, "Micro-light-emitting diodes with quantum dots in display technology," Light Sci. Appl. **9**, 91 (2020).
2. H. Zhang, Q. Su, and S. Chen, "Recent progress in the device architecture of white quantum-dot light-emitting diodes," J. Inf. Disp. **20**, 169–180 (2019).
3. H. J. Jang, J. Y. Lee, J. Kim, J. Kwak, and J. H. Park, "Progress of display performances: AR, VR, QLED, and OLED," J. Inf. Disp. **21**, 1–9 (2020).
4. J. J. Wierer, N. Tansu, A. J. Fischer, and J. Y. Tsao, "III-nitride quantum dots for ultra-efficient solid-state lighting," Laser Photon. Rev. **10**, 612–622 (2016).
5. S. Fafard, K. Hinzer, and C. N. Allen, "Semiconductor quantum dot nanostructures and their roles in the future of photonics," Braz. J. Phys. **34**, 550–554 (2004).
6. B. Tongbram, H. Ghadi, S. Adhikary, A. Mandal, and S. Chakrabarti, "Cross-sectional TEM (XTEM) analysis for vertically coupled quaternary $In_{0.21}Al_{0.21}Ga_{0.58}As$ capped InAs/GaAs quantum dot infrared photodetectors," Proc. SPIE **9373**, 93730S (2015).
7. D. Yan, S. Zhao, Y. Zhang, H. Wang, Z. Zang, D. Yan, S. Zhao, Y. Zhang, H. Wang, and Z. Zang, "High efficient emission and high-CRI warm white light-emitting diodes from ligand-modified $CsPbBr_3$ quantum dots," Opto-Electron. Adv. **4**, 200075 (2021).
8. D. Yan, T. Shi, Z. Zang, T. Zhou, Z. Liu, Z. Zhang, J. Du, Y. Leng, and X. Tang, "Ultrastable $CsPbBr_3$ perovskite quantum dot and their enhanced amplified spontaneous emission by surface ligand modification," Small **15**, 1901173 (2019).
9. Q. Mo, C. Chen, W. Cai, S. Zhao, D. Yan, and Z. Zang, "Room temperature synthesis of stable zirconia-coated $CsPbBr_3$ nanocrystals for white light-emitting diodes and visible light communication," Laser Photon. Rev. **15**, 2100278 (2021).
10. S. K. Karunakaran, G. M. Arumugam, W. Yang, S. Ge, S. N. Khan, Y. Mai, X. Lin, and G. Yang, "Europium (II)-doped all-inorganic $CsPbBr_3$ perovskite solar cells with carbon electrodes," Sol. RRL **4**, 2000390 (2020).
11. D. G. Deppe, L. A. Graham, and D. L. Huffaker, "Enhanced spontaneous emission using quantum dots and an apertured microcavity," IEEE J. Quantum Electron. **35**, 1502–1508 (1999).
12. D. L. Huffaker, G. Park, Z. Zou, O. B. Shchekin, and D. G. Deppe, "1.3 μm room-temperature GaAs-based quantum-dot laser," Appl. Phys. Lett. **73**, 2564–2566 (1998).
13. A. Stintz, G. T. Liu, H. Li, L. F. Lester, and K. J. Malloy, "Low-threshold current density 1.3-μm InAs quantum-dot lasers with the dots-in-a-well (DWELL) structure," IEEE Photon. Technol. Lett. **12**, 591–593 (2000).
14. J. M. Ferreyra and C. R. Proetto, "Strong-confinement approach for impurities in quantum dots," Phys. Rev. B **52**, R2309–R2312 (1995).
15. Y. Arakawa and H. Sakaki, "Multidimensional quantum well laser and temperature dependence of its threshold current," Appl. Phys. Lett. **40**, 939–941 (1982).
16. I.-K. Park, M.-K. Kwon, C.-Y. Cho, J.-Y. Kim, C.-H. Cho, and S.-J. Park, "Effect of InGaN quantum dot size on the recombination process in light-emitting diodes," Appl. Phys. Lett. **92**, 253105 (2008).
17. C. H. Lu, Y. C. Li, Y. H. Chen, S. C. Tsai, Y. L. Lai, Y. L. Li, and C. P. Liu, "Output power enhancement of InGaN/GaN based green light-emitting diodes with high-density ultra-small In-rich quantum dots," J. Alloys Compd. **555**, 250–254 (2013).
18. W. Lv, L. Wang, J. Wang, Z. Hao, and Y. Luo, "InGaN/GaN multilayer quantum dots yellow-green light-emitting diode with optimized GaN barriers," Nanoscale Res. Lett. **71**, 617 (2012).
19. T. Frost, A. Banerjee, K. Sun, S. L. Chuang, and P. Bhattacharya, "InGaN/GaN quantum dot red (λ = 630 nm) laser," IEEE J. Quantum Electron. **49**, 923–931 (2013).
20. Y. Mei, G.-E. Weng, B.-P. Zhang, J.-P. Liu, W. Hofmann, L.-Y. Ying, J.-Y. Zhang, Z.-C. Li, H. Yang, and H.-C. Kuo, "Quantum dot vertical-cavity surface-emitting lasers covering the 'green gap'," Light Sci. Appl. **61**, e16199 (2016).
21. B. Damilano, N. Grandjean, S. Vézian, and J. Massies, "InGaN heterostructures grown by molecular beam epitaxy: from growth mechanism to optical properties," J. Cryst. Growth **227–228**, 466–470 (2001).
22. C. Bayram and M. Razeghi, "Stranski–Krastanov growth of InGaN quantum dots emitting in green spectra," Appl. Phys. A **96**, 403–408 (2009).
23. C. Adelmann, J. Simon, N. T. Pelekanos, Y. Samson, G. Feuillet, and B. Daudin, "Growth and optical characterization of InGaN quantum dots resulting from a 2D–3D transition," Phys. Status Solidi **176**, 639–642 (1999).
24. B. Damilano, N. Grandjean, S. Dalmasso, and J. Massies, "Room-temperature blue-green emission from InGaN/GaN quantum dots made by strain-induced islanding growth," Appl. Phys. Lett. **75**, 3751–3753 (1999).
25. S. Figge, C. Tessarek, T. Aschenbrenner, and D. Hommel, "InGaN quantum dot growth in the limits of Stranski–Krastanov and spinodal decomposition," Phys. Status Solidi **248**, 1765–1776 (2011).
26. F. Ivaldi, C. Meissner, J. Domagala, S. Kret, M. Pristovsek, M. Högele, and M. Kneissl, "Influence of a GaN cap layer on the morphology and the physical properties of embedded self-organized InN quantum dots on GaN(0001) grown by metal–organic vapour phase epitaxy," Jpn. J. Appl. Phys. **50**, 031004 (2011).
27. Q. Wang, T. Wang, J. Bai, A. G. Cullis, P. J. Parbrook, and F. Ranalli, "Influence of annealing temperature on optical properties of InGaN quantum dot based light emitting diodes," Appl. Phys. Lett. **93**, 081915 (2008).
28. S. Liu, J. Yang, D. Zhao, D. Jiang, J. Zhu, F. Liang, P. Chen, Z. Liu, Y. Xing, L. Peng, and L. Zhang, "Uniform-sized indium quantum dots grown on the surface of an InGaN epitaxial layer by a two-step cooling process," Nanoscale Res. Lett. **14**, 280 (2019).
29. A. Kadir, C. Meissner, T. Schwaner, M. Pristovsek, and M. Kneissl, "Growth mechanism of InGaN quantum dots during metalorganic vapor phase epitaxy," J. Cryst. Growth **334**, 40–45 (2011).

30. L. Wang, L. Wang, C.-J. Chen, K.-C. Chen, Z. Hao, Y. Luo, C. Sun, M.-C. Wu, J. Yu, Y. Han, B. Xiong, J. Wang, and H. Li, "Green InGaN quantum dots breaking through efficiency and bandwidth bottlenecks of micro-LEDs," Laser Photon. Rev. **15**, 2000406 (2021).
31. G. Liu, H. Zhao, J. Zhang, J. H. Park, L. J. Mawst, and N. Tansu, "Selective area epitaxy of ultra-high density InGaN quantum dots by diblock copolymer lithography," Nanoscale Res. Lett. **61**, 342 (2011).
32. Y. K. Ee, H. Zhao, R. A. Arif, M. Jamil, and N. Tansu, "Self-assembled InGaN quantum dots on GaN emitting at 520 nm grown by metalorganic vapor-phase epitaxy," J. Cryst. Growth **310**, 2320–2325 (2008).
33. X. Xiao, A. J. Fischer, G. T. Wang, P. Lu, D. D. Koleske, M. E. Coltrin, J. B. Wright, S. Liu, I. Brener, G. S. Subramania, and J. Y. Tsao, "Quantum-size-controlled photoelectrochemical fabrication of epitaxial InGaN quantum dots," Nano Lett. **14**, 5616–5620 (2014).
34. X. Xiao, A. J. Fischer, M. E. Coltrin, P. Lu, D. D. Koleske, G. T. Wang, R. Polsky, and J. Y. Tsao, "Photoelectrochemical etching of epitaxial InGaN thin films: self-limited kinetics and nanostructuring," Electrochim. Acta **162**, 163–168 (2015).
35. X. Wei, S. A. Al Muyeed, M. R. Peart, W. Sun, N. Tansu, and J. J. Wierer, "Room temperature luminescence of passivated InGaN quantum dots formed by quantum-sized-controlled photoelectrochemical etching," Appl. Phys. Lett. **113**, 121106 (2018).
36. S. A. Al Muyeed, X. Wei, D. Borovac, R. Song, N. Tansu, and J. J. Wierer, "Controlled growth of InGaN quantum dots on photoelectrochemically etched InGaN quantum dot templates," J. Cryst. Growth **540**, 125652 (2020).
37. S. A. Al Muyeed, W. Sun, X. Wei, R. Song, D. D. Koleske, N. Tansu, and J. J. Wierer, "Strain compensation in InGaN-based multiple quantum wells using AlGaN interlayers," AIP Adv. **7**, 105312 (2017).
38. C. B. Soh, W. Liu, S. J. Chua, R. J. N. Tan, S. S. Ang, and S. Y. Chow, "Red emitting LEDs formed by indium rich quantum dots incorporated in MQWs," Phys. Status Solidi **208**, 1579–1581 (2011).
39. S. Saito, R. Hashimoto, J. Hwang, and S. Nunoue, "InGaN light-emitting diodes on *c*-face sapphire substrates in green gap spectral range," Appl. Phys. Express **6**, 111004 (2013).
40. D. D. Koleske, A. J. Fischer, B. N. Bryant, P. G. Kotula, and J. J. Wierer, "On the increased efficiency in InGaN-based multiple quantum wells emitting at 530–590 nm with AlGaN interlayers," J. Cryst. Growth **415**, 57–64 (2015).
41. S. L. Chuang and N. Holonyak, Jr., "Efficient quantum well to quantum dot tunneling: analytical solutions," Appl. Phys. Lett. **80**, 1270–1272 (2002).
42. I. Vurgaftman, J. R. Meyer, and L. R. Ram-Mohan, "Band parameters for III-V compound semiconductors and their alloys," J. Appl. Phys. **89**, 5815–5875 (2001).
43. O. Ambacher, J. Majewski, C. Miskys, A. Link, M. Hermann, M. Eickhoff, M. Stutzmann, F. Bernardini, V. Fiorentini, V. Tilak, B. Schaff, and L. F. Eastman, "Pyroelectric properties of Al(In)GaN/GaN hetero- and quantum well structures," J. Phys. Condens. Matter **14**, 3399–3434 (2002).